Clemson University
TigerPrints

All Theses   Theses

12-2010

THE DEPENDENCE OF ELECTRICAL RESISTIVITY, SATURATION AND SATURATION EXPONENT ON MULTI-PHASE FLOW INSTABILITY

Zuolin Liu
Clemson University, jeolinliu@gmail.com

Follow this and additional works at: https://tigerprints.clemson.edu/all_theses

Part of the Hydrology Commons

THE DEPENDENCE OF ELECTRICAL RESISTIVITY, SATURATION AND SATURATION
EXPONENT ON MULTI-PHASE FLOW INSTABILITY

A Thesis
Presented to
the Graduate School of
Clemson University

In Partial Fulfillment
of the Requirements for the Degree
Master of Science
Hydrogeology

by
Zuolin Liu
December 2010

Accepted by:
Stephen Moysey, Committee Chair
Ronald W. Falta
Brian A. Powell

Abstract

   Multiphase flow channeling in oil reservoirs during water floods reduces oil

recovery. Electrical methods may be used to monitor reservoirs and detect the onset

of channeling, but the dependence of electrical resistivity on reservoir flow conditions

is complex. The present study is directed toward understanding how the parameters

of Archie's law, a commonly assumed relationship between electrical resistivity and

water saturation in a porous medium, depends on multiphase flow instability leading

to flow channeling. In this research a series of 34 flow experiments were conducted

in a thin, two-dimensional tank (55cm x 55cm x 3.75cm) packed with 2mm glass

beads where mineral oil was displaced by Nigrosine dyed water. The tank was

designed to tilt to arbitrary angles, thereby allowing experiments to be conducted for

different values of the generalized Bond number, which describes the overall balance

between viscous, capillary, and gravity forces affecting flow instability, by varying

the water application rate and orientation of the tank. The effective electrical

resistivity of the tank was measured continuously during the flow experiments using a

National Instruments digital multi-meter (NI PXI-4071 7 1/2 Digit Flex DMM).

Concurrently, a light transmission method was used to monitor spatial variations of

oil and water saturation in the tank using a digital camera. The saturation images

were then used to derive the average tank saturation over time. The resistivity index

derived from Archie's law generally decreases as the water saturation increases in the

tank and sharp drops are observed when individual fingers of water span the entire tank to create a continuous electrically conductive pathway. The magnitude of this resistivity index drop decreases when the displacement pattern becomes more unstable and disappears under highly unstable flow conditions. Based on the resistivity and saturation data, the saturation exponent in Archie's law was estimated over the course of the experiment for each set of experimental conditions. The saturation exponent increases as the water displaces oil and reaches a constant value after water breakthrough occurs and a stable flow pattern is established. At equilibrium, the saturation exponent increases from 0.65 to 1.94 as the generalized Bond number is decreased to transition between stable and unstable flow conditions. The saturation exponent remains constant at 1.94 when the flow is unstable for generalized Bond numbers less than -0.106.

Table of Contents

Table of Contents (Continued)

List of Figures

List of Tables

Chapter 1 Introduction

1.1 Motivation for this research

Multi-phase flow in porous media occurs for a wide range of problems including petroleum production (Mogensen et al., 2001; Tiab et al., 2004), non-aqueous phase liquid (NAPL) contamination and remediation (Aggelopolos et al., 2005; Bradford et al., 1999; Schroth et al., 1995; Steenhuis et al., 1997; Villaume et al., 1985; Weisbrod et al., 2002; Zhang et al., 2002) and CO_2 sequestration (Christensen et al. 2006). The complex flow behavior of immiscible fluids has been studied at the pore scale (Lenormand, 1990; Mogensen et al., 2001), in one dimensional columns (Aggelopolos et al., 2005; Bradford et al., 1999) using multidimensional flow cells (Darnault et al., 1998; Mdheust et al., 2002; Steenhuis et al., 1997) by laboratory experiments. In particular, the occurrence of preferential flow paths during oil recovery causes short circuiting of viable reserves during water floods. Identifying flow channeling in reservoirs is therefore essential for proper assessment of reserves when determining the efficiency of oil recovery.

Electromagnetic (EM) methods have been widely used for investigating multiphase flow during reservoir water floods and steam floods (Christos et al., 1998; Man et al., 2000; Moss et al., 2002; Tiab et al., 2004; Zhou et al., 1997), CO_2 sequestration (Christensen et al., 2006), and unsaturated flow in the vadose zone (Aggelopolos et al., 2005; Bekri et al., 2003; Blunt et al., 2002). Archie (1942) derived an empirical relationship between water saturation and electrical resistivity in reservoir rocks based on the experimental data which is widely used to interpret the logging data to estimate the hydrocarbon reserves for a given formation. The

influence of flow channeling on the apparent electrical resistivity measured using EM surveys must be better understood to quantitatively interpret changes in saturation using this geophysical monitoring data. Specifically, flow channeling effects on the parameters of Archie's Law need to be investigated to improve the accuracy of resistivity data interpretation.

1.2 Background

1.2.1 Channeling in multiphase flow

In immiscible two phase flows, variations of stable and unstable flow behavior have been observed during the displacement process (Aggelopoulos et al., 2005; Bauters et al., 1998; Catalan et al., 1995; Lenormand, 1990; Løvoll et al., 2005; Méheust et al., 2002; Rimmer et al., 1996; Steenhuis et al., 1997; Stokes et al., 1986; Weisbrod et al., 2002). Key variables affecting flow behavior include the fluid flow rates, viscosities and densities of fluids, wettability of grains, and characteristics of the pore space. In this study we consider a situation where a wetting fluid with high density invades, from below, a porous medium initially saturated by a less dense nonwetting phase. The wetting phase is less viscous than nonwetting phase. At very low flow rates, the viscous pressure drop is negligible compared to the capillary pressure threshold (Lenormand, 1990). The displacement results are controlled by capillary and gravity effects. However, at high flow rates viscous forces dominate the capillary effect, because the defending phase is more viscous. The competition between gravitationally stable and viscous forces contributes to the instability of the flow. The hydrostatic gradient created by gravitational forces will stabilize the

wetting fluid motion, while the viscous force tends to destabilize the front (Løvoll et al., 2005; Méheust et al., 2002). The degree to which these two forces are imbalanced will dictate whether preferential flow via viscous fingering will occur.

Oostrom et al. (2007) provided a literature review of 2- and 3-dimensional multiphase flow experiments in the laboratory at the intermediate scale that focused on issues including flow behavior, saturation imaging and tracer detection, and quantification of multi-phase flow. Most previous experiments were conducted in water-wet glass beads or silica sands and a variety of techniques were used for the measurement of liquid saturation, including: synchrotron X-ray attenuation (Steenhuis et al., 1997), X-ray CT scanning (Mogensen et al., 2001) and light transmission (Dicarlo et al., 1997; Méheust et al., 2002; Steenhuis et al., 1997; Weisbrod et al., 2002). Of these techniques, the light transmission method has the fewest requirements for specialized equipment and also has the lowest cost. In the light transmission method, a light source is placed on one side of the flow tank and the intensity of light traveling through the tank is measured using a camera. When one of the fluid phases is dyed, the intensity of the transmitted light can be correlated to fluid saturation, thereby allowing the distribution of fluid saturation in the tank to be mapped at the pixel scale within the image.

1.2.2 Archie's Law

In rocks with grains that are not electrically conductive, electrical current is primarily carried by the aqueous solution filling the pore space. In this case, Archie's law (1942) is commonly used to capture the resulting relationship between the porosity (ϕ) and measured bulk resistivity of a water saturated rock (ρ_b). In equation

1 the parameters *a* and *m* are empirical constants related to the geometry and connectivity of the pore space. The overall influence of the pore network on resistivity is captured by the formation factor (F_f) of a rock, which is defined as the ratio of the bulk rock resistivity to the resistivity of the fluid filling the pore space (ρ_o).

$$\rho_b = a\phi^{-m}\rho_o = F_f\rho_o \tag{1}$$

When a second, non-conductive fluid is also present in the rock, pore water continues to carry the electrical current but the entire volume of the pore space is no longer available for current flow. The resulting increase in resistivity is accounted for in Archie's law by including a term quantifying the degree of water saturation (S_w) in the medium and including an additional empirical constant, n, as shown in equation 2. This equation has been widely used to interpret electrical logging to estimate reservoir oil reserves (Archie, 1942; Bekri et al., 2003; Ingham et al., 2008; Man et al., 2000; Tsakiroglou et al., 1999)).

$$\rho_b = a\phi^{-m}\rho_o\, S_w^{-n} \tag{2}$$

Analogous to the single phase case, the saturation exponent (*n*) captures the connectivity of the electrically conductive phase in the porous medium, i.e., the water phase. The ratio of the bulk resistivity of a partially saturated rock, i.e., $\rho_b\,(S_w{\neq}1)$, to the resistivity of a 100% water saturated rock, i.e., $\rho_b(S_w{=}1)$, is commonly known as the resistivity index (I_R).

$$I_R = \frac{\rho_b(S_w\neq1)}{\rho_b(S_w=1)} = \frac{a\phi^{-m}\rho_o S_w^{-n}}{a\phi^{-m}\rho_o} = S_w^{-n} \tag{3}$$

Although Archie's Law is widely used, it is not always valid because resistivity depends on the wettability, saturation history and content of clay minerals (Zhou et al., 1997). The geometry of the conductive phase is another major issue that can affect

4

Archie's law since the relative distribution of oil and water in the subsurface depends on the flow conditions and management history of the reservoir.

Quantifying how the flow conditions within a reservoir affect the parameters of Archie's law is an important problem for interpreting reservoir saturations from resistivity surveys of dynamic flow systems. In particular, flow instability caused by the cumulative effects of capillary, gravity, and viscous forces can lead to fingering of the conductive water phase through the resident non-conductive oil phase. Viscous fingering increases the residual oil volume in the reservoir (Løvoll et al., 2005) while significantly reducing the bulk resistivity of the reservoir. Using column experiments Aggelopolos et al. (2005) showed that fingering during unstable flow has a strong effect on the resistivity index. To date, however, there has been limited work focused on understanding whether the saturation exponent in Archie's law can be directly linked to parameters used to quantify flow instability, such as the Capillary and Bond numbers. Aggelopolos et al. (2005) found that the saturation exponent decreases as the displacement front advances in destabilized drainage and at very high absolute values of the Bond number the saturation exponent may be constant and independent of water saturation. Despite these efforts, the dependence of saturation exponent on the instabilities caused by viscous fingering still needs to be developed.

1.3 Thesis Overview

The main objective of this research is to test the hypothesis that there is a relationship between parameters describing flow instability, i.e., capillary and Bond number, and the electrical properties of the porous medium, specifically the saturation exponent in Archie's law. To achieve this goal, a multiphase flow experiment using

water and mineral oil was conducted in a two-dimensional tank packed with glass beads. A Digital Multi-meter was used to measure the bulk resistivity of the tank over the course of the experiment while a camera simultaneously monitored the distribution of Nigrosine dyed water as it displaced the initially saturating oil phase. Flow conditions in the tank were varied by controlling the water injection rate and orientation of the tank. The measured real time resistivity index curves and saturations, which are derived from the image data, are used to calculate the saturation exponent for each set of experimental conditions. The relationship between Archie's saturation exponent and flow condition is then found.

The motivation for this research is given in Chapter 1 (this chapter). The materials, methods, experiments setup and summary of all experiments performed are given in Chapter 2. Chapter 3 presents the resistivity and saturation data of all experiments. An overview of the conclusions from this work and suggestions for future work are given in Chapter 4. Details of the experimental protocols are summarized in the appendices of this thesis.

Chapter 2 Experimental Methods

An experimental apparatus (Figure 2.1) was constructed to dynamically measure electrical resistivity in a porous medium while simultaneously imaging the distribution of oil and water during a series of water flood experiments. The apparatus is unique in that it was designed to tilt to arbitrary angles (φ), thereby providing a means to control the influence of gravity in the experiments.
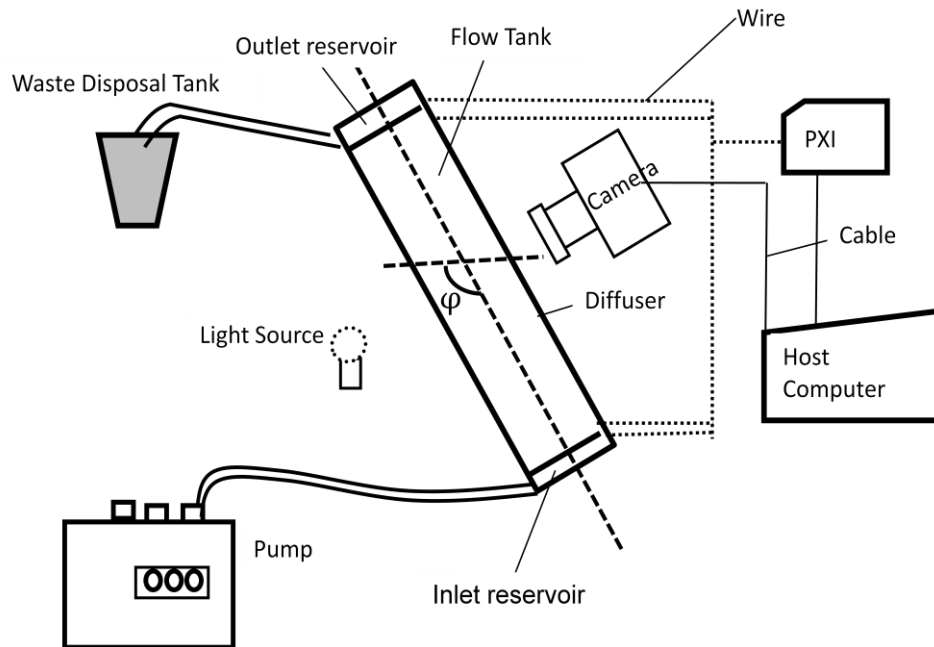
Figure 2.1 A sketch of the experimental setup (side profile of tank).

In all the experiments, a 2-dimensional (55cm x 55cm x 3.75cm) acrylic flow tank is packed with 2 mm glass beads (Walter Stern). The tank was manually shaken during packing to homogenize the media. Water with dye (Nigrosine, Acros Organics) was injected to the tank to displace mineral oil. Properties of the fluids are given in Table 3.1 (Chapter 3). During each experiment a pump supplied a constant flux of water to an internal reservoir separated from the main tank by a plastic diffuser

(Figure 2.1) filled with many small 1/8" holes in an effort to distribute flow evenly in the tank. The outlet also consisted of a reservoir separated from the flow cell by a thin plastic diffuser. The end of the tubing carrying fluid away from the outlet reservoir was kept at a constant elevation across experiments to provide a constant positive pressure boundary at the outlet of the tank.

2.1 Electrical measurement

Four pieces of copper mesh are fixed on the both sides of the two-dimensional acrylic flow cell to measure 4-wire resistance using a digital multi-meter (NI PXI-4071 7 1/2 Digit FlexDMM, DMM), which is installed in one slot of the NI PXI-1033 Chassis (Figure 2.3). The two outer electrodes are connected to apply a uniform DC electrical current. The other two electrodes are used to measure the average potential across the tank. Rather than directly feeding the electrodes to the DMM, they are led to a NI PXI-2530 High-Density Multiplexer/Matrix Switch placed in another slot of the NI PXI-1033 Chassis. The matrix switch allows for switching between the positive electrode and negative electrode in order to reduce polarization effects at the electrodes.
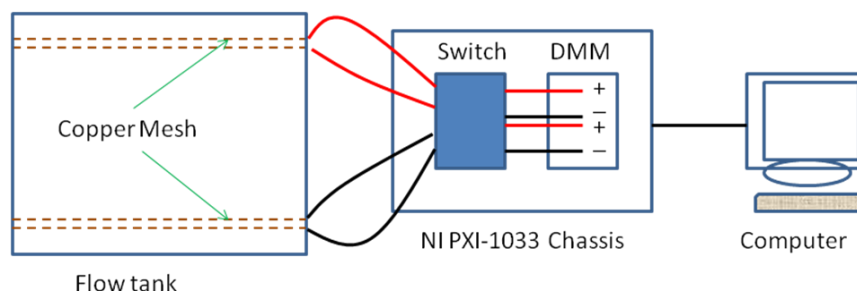
Figure 2.2 Electrical apparatus (front view of the tank)

During the experiments the real time resistance is shown in the LABVIEW front

panel and logged to a data file. The polarity switching causes the measurements to be reported as both positive and negative resistance. The average of the absolute value of negative resistance (R_-) and positive resistance (R_+) was used to calculate resistivity by:

$$\rho_w = \frac{(R_- + R_+)A}{2L} \tag{1}$$

Where A is the cross-section area (45cm x 1.25cm) which is perpendicular to the direction of electrical current, and L is the distance between two potential electrodes.
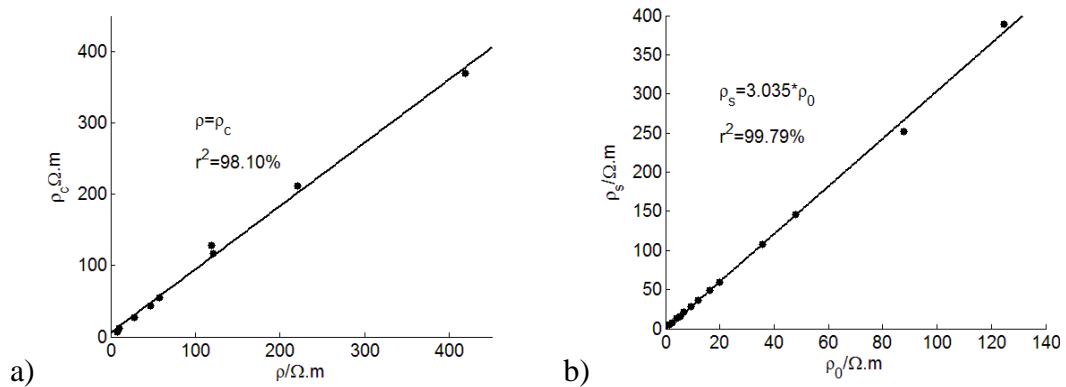
Figure 2.3 a) Calibration of DMM, Relationship between resistivity from conductivity meter (ρ_0) and DMM (ρ); b) Formation factor

To calibrate our apparatus the unpacked tank was filled with different saline solutions and the resistivity are measured by the DMM and compared with those measured using a standard fluid conductivity meter (VWR sympHony SP90M5 Handheld meter). Figure 2.3a shows the resistivity of water in the tank measured by the DMM (given L=32cm and A=45x1.25 cm^2), compared to the resistivity measured by a conductivity meter in a beaker. These two dataset matches have an agreement with a R^2 of 0.98.

To determine the formation effect on the electrical resistivity in the porous media, we measure the formation factor (F_f). Figure 2.3b shows the relationship between resistivity of water-saturated glass beads (ρ_s) and the resistivity of the water (ρ_0). The slope indicates that the formation factor is 3.035 with R^2 of 99.79% at the porosity of 0.28 when the tank was packed with 2mm glass beads. For calculating the resistivity index (I_R), we use the DMM to measure $\rho_b(S_w \neq 1)$ and a conductivity meter to measure water resistivity (ρ_0), and multiply by formation factor (Ff) to get $\rho_b(S_w = 1)$, the resistivity of the glass beads at 100% water saturation (Equation 1, 2 ,3 in Chapter 1) . This curve needs to be calibrated if different porosity, particle material and size are used.

2.2 Saturation acquisition

To image changes in saturation, a camera (DFK 41BU02.H USB CCD, Imaging Source) was affixed to a bracket 40 cm in front of the tank. The bracket allowed the camera to remain in the same position relative to the tank regardless of the tank orientation. A total of six fluorescent bulbs were affixed to the back of the tank to generate the transmitted light for saturation measurements. A diffuser is installed in the between the tank and lights which is used to help distribute the light as evenly as possible across the tank. The resolution of the camera is 1280 x 960, which provides a spatial resolution of 0.39 mm per pixel or about 2 pixels per pore.

As both the water and mineral oil phases in our fluid system are usually clear liquids, the water is dyed by Nigrosine to enhance the visual contrast. Initial batch experiments in a beaker showed that the dye did not bleed between the water and oil phase. To find an appropriate amount of dye to acquire excellent quality images,

several concentrations of Nigrosine solution were tested. We found that a concentration of 0.05g/L provided good quality images.

To test the light transmission technique and obtain a calibration curve between the light intensity and water saturation, a small chamber was built with the same material and thickness as the flow cell. Figure 2.4 shows the pictures of the light transmission through this chamber, packed with the same glass beads used in the flow experiments. For the calibration, the beads were packed to give a porosity of 0.28. Water was added to the test cells in sufficient amount to ultimately provide water saturations of 0, 0.2, 0.4, 0.6, 0.8, and 1. The remaining of the pore space was filled with mineral oil. Each water saturation condition was created by measuring the appropriate volume of each phase in a graduate cylinder and then pouring them into the test chamber uniformly and carefully to avoid air bubbles. At each saturation, the color is not completely uniform, spatial differences exist since water and oil are immiscible.
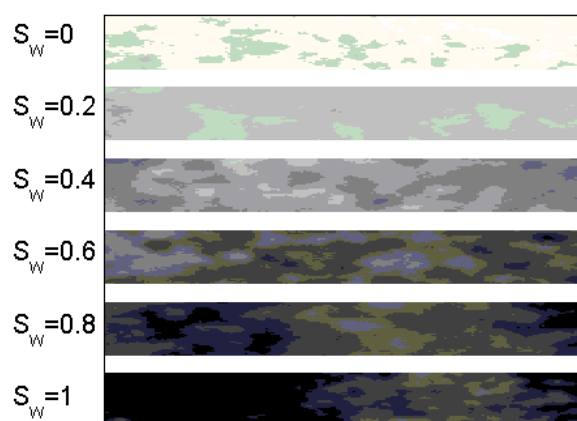
Figure 2.4 A picture of the calibration chamber, with cells filled with varying water saturation

The RGB value of the images is converted into gray scale using MATLAB (Version 6, MathWorks), get the intensity (I) of each pixel and take the average gray

scale value of the entire chamber. This is 180 x 62 pixels as the gray scale value of the corresponding saturation. For avoiding the inaccuracy of changing camera settings, we use the intensity of S_w=0 as reference (I_0). The intensity of specific saturation is the gray scale value of that saturation subtracted from I_0 at S_w=0. These values are plotted versus the corresponding water saturation to obtain a calibration curve shown in Figure 2.5.
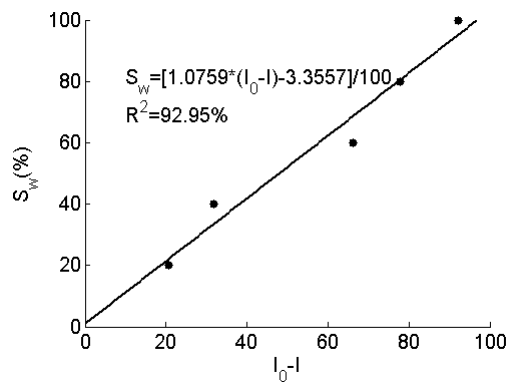
Figure 2.5 Relationship between the transmitted light Intensity and water saturation in glass beads formation with porosity of 0.28

Color differences are visible between the different saturations (Figure 2.4); the degree of black represents the amount of water and oil is white in the chamber. The intensity (I_0-I) values increase with the water content and a linear regression provided a good fit with R^2 of 92.95% (Figure 2. 5). The (I_0-I)-S_w equation is:

$$S_w=[1.0759(I_0\text{-}I)\text{-}3.3557]/100 \tag{2}$$

Where S_w is the water saturation and I is the pixel intensity of the picture. The system needs to be calibrated when using a different video camera or particle material and sizes.

12

Equation 2 is used to calculate the water saturation of each pixel. The average pixel saturation is used to obtain the water saturation of the entire tank corresponding to the resistance at specific time.

Chapter 3 The Dependence of Electrical Resistivity-Saturation Relationships on Multi-Phase Flow Instability

Abstract

Multiphase channeling in reservoirs as a result of flow instability is an important cause of poor oil recovery. The present study is directed toward understanding how the parameters of Archie's law, a commonly assumed relationship between electrical resistivity and water saturation in a porous medium, depends on multiphase flow instability. Flow experiments were conducted in a thin, two-dimensional tank (55cm x 55cm x 3.75cm) packed with 2 mm glass beads where mineral oil was displaced by Nigrosine dyed water. Multiphase flow behavior is investigated using the light transmission method and electrical resistivity measurements. Different experiments were performed by varying the water application rate and orientation of the tank to control the generalized Bond number, which describes the balance between viscous, capillary, and gravity forces that affect flow instability. The experimental results show that overall the resistivity index gradually decreases as water saturation increases in the tank, but drops sharply as individual capillary fingering fronts reach the outlet to create a high-conductivity pathway that bridges the tank. The magnitude of this drop decreases as the displacement becomes increasingly unstable and disappears for highly unstable flow leading to the generation of many small fingers. At flow equilibrium, we found that the saturation exponent increases from 0.65 to 1.94 as the flow becomes increasingly unstable until it reaches a constant value of

1.94 for values of the generalized Bond number less than -0.106.

3.1 Introduction

Multiphase fluid flow in porous media is an important problem for applications ranging from petroleum production (Mogensen et al., 2001; Tiab et al., 2004), to the migration of non-aqueous phase liquids (NAPLs) in soils and aquifers (Aggelopolos et al., 2005; Bradford et al., 1999; Schroth et al., 1995; Steenhuis et al., 1997; Villaume et al., 1985; Weisbrod et al., 2002; Zhang et al., 2002) and CO_2 sequestration (Christensen et al, 2006). Viscous, capillary and gravity forces interact in immiscible two phase flow systems to produce stable or unstable flow regimes (Méheust et al., 2002; Løvoll et al., 2005). In a stable flow regime the displacement of one fluid for another will occur along a stable front. In unstable flow regimes, fingering can occur along the displacement front. As a result, the invading fluid can bypass significant amounts of the original fluid phase, leaving it in place in the medium.

Electrical resistivity measurements are commonly used to investigate fluid saturations in multiphase flow systems (Bekri et al., 2003; Blunt et al., 2002; Moss et al., 2002; Zhou et al., 1997). The resistivity index provides an expression of resistivity for multi-phase flow systems that is directly related to the degree of water saturation of the medium, S_w, through Archie's law (Archie, 1942). The resistivity index I_R is equal to the ratio of the resistivity of the sample (ρ_w) measured at saturation S_w to the resistivity of the sample measured at 100% water saturation (ρ_s) (Equation 1). The saturation exponent, n, is an empirical constant that is conceptually related to the connectivity of the electrically conductive phase, i.e., water.

The saturation exponent, which is ranging between 1.9 and 3.5 for intermediate wet systems (Zhou et al., 1997), is usually determined experimentally from measurements of I_R and S_w using equation 1. Sweeney and Jennings (1960) found the saturation exponent to be about 1.9 on neutrally-wet systems. Although Archie's Law is widely used to determine fluid saturation from resistivity measurements, it is not always valid as the saturation-resistivity relationship depends on the wettability, saturation history, content of clay minerals and salinity of the brine phase (Anderson, 1989; Sharma et al., 1991; Moss, 1999; Moss et al., 2002; Zhou et al., 1997). Resistivity measurements may, also be sensitive to differences in the arrangement of oil and water for stable versus unstable flow systems, thereby making the interpretation of saturation dependent on the flow regime.

$$I_R = \frac{\rho_w}{\rho_s} = S_w^{-n} \tag{1}$$

Experimentally investigate the influence of flow instability on the saturation exponent in Archie's law. To this end, multiphase flow experiments are conducted where water is used to displace mineral oil in a 2D flow system. A series of experiments is conducted in which the stability of the flow is controlled by varying the water inflow rate and angle of the tank. The measurements of the bulk resistivity of the tank are obtained during the flow experiments. Concurrently, transient measurements of average water saturation in the tank, S_w, are derived from video collected using the light transmission method. From these measurements, whether there is a dependence of the saturation exponent in Archie's law on the flow conditions in a porous medium is evaluated.

3.2 Background: Flow channeling in reservoirs

It is well known that variations in the magnitude and connectivity of permeability could lead flow channeling in reservoirs and reduce oil production (Hovadik et al., 2007). Even in a homogeneous medium, however, flow instability can cause viscous fingering that also increases the residual oil volume left behind in a reservoir (Løvoll et al., 2005). Flow instability is affected by the cumulative effects of capillary, buoyancy, and viscous forces. Viscous forces can destabilize the displacement front into narrow fingers if less viscous fluid is displacing a more viscous fluid, whereas gravity plays a stabilizing effect when the light fluid is on the top of denser phase (Méheust et al., 2002). This type of fingering can occur when the viscosity of the displaced fluid is greater than that of the injected fluid. The balance between forces in a two-phase flow system can be quantified using the dimensionless Bond and Capillary numbers along with the viscosity ratio. The viscosity ratio (*M*) is defined as the viscosity of displacing fluid μ_w divided by the viscosity of the displaced fluid μ_n. The viscous fingering can be observed when viscous ratio is less than 1 at fast displacement, and the viscous force overcome capillary and gravity effect.

The Bond number (B_o), given in Equation 2, expresses the relative importance of gravitational to capillary forces in a multiphase flow system at pore scale (Méheust et al., 2002; Løvoll et al., 2005). In contrast, the Capillary number (C_a) in Equation 3 expresses the balance between viscous to capillary forces at pore level (Méheust et al., 2002; Løvoll et al., 2005).

$$B_o = \frac{\Delta P_{grav}}{\Delta P_{cap}} = \frac{\Delta \rho g a^2}{\gamma} \sin\varphi \qquad\qquad (2)$$

$$Ca = \frac{\Delta P_{visc}}{\Delta P_{cap}} = \frac{\mu_w v a^2}{\gamma k} \qquad (3)$$

In these expressions μ_w is the viscosity of wetting fluid, v is the filtration or Darcy velocity, a is the typical pore size, γ is surface tension, $\Delta\rho$ is the density difference between the two fluids, g is the acceleration due to the gravity, φ is the angle of flow relative to horizontal, and k is the permeability of the porous medium (Løvoll et al., 2005; Méheust et al, 2002). The capillary and Bond numbers can be combined to produce the generalized Bond number (B_o^*) given in Equation 4 (Løvoll et al., 2005; Méheust et al., 2002).

$$B_o^* = B_o - C_a = \frac{a^2}{\gamma k}(\Delta\rho g k \sin\varphi - \mu_w v) \qquad (4)$$
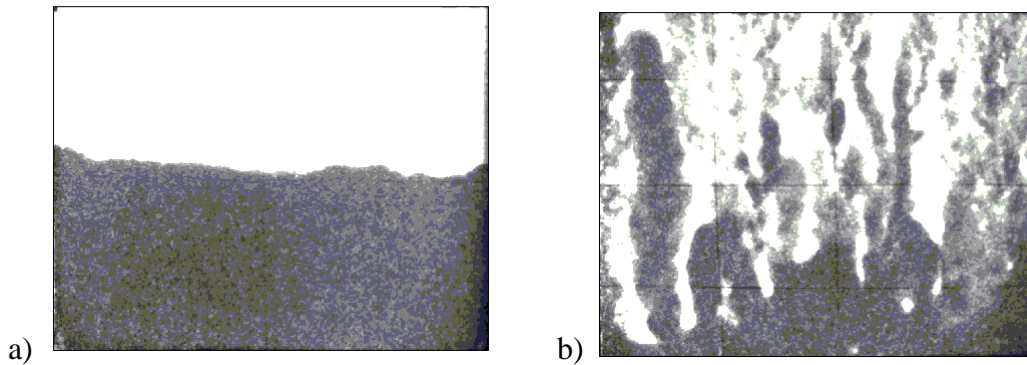
Figure 3.1 Comparison of a) stable flow conditions (B_o^*=0.00612) and b) unstable flow conditions (B_o^*=-0.248) for oil (white) displaced by Nigrosine dyed water (dark)

The value of the generalized Bond number plays a critical role for determining the occurrence of viscous instabilities. For $B_o^* > 0$ fingering occurs as a compact and flat front that is described as stable flow as illustrated in Figure 3.1a. However, when $B_o^* < 0$ the flow is unstable and fingering produces an uneven and often rapid movement of the infiltrating phase through the displaced phase in porous medium (Figure 3.1b).

The white region in the images corresponds to oil, whereas the black areas correspond to Nigrosine dyed water. The transition zone between stable and unstable displacement does not consist of a radical change in the local dynamics of the interface (Løvoll et al., 2005; Méheust et al., 2002).

3.3 Methods and Experimental setup

The main goal of this work is to determine the relationship between the saturation exponent in Archie's law and the degree of flow instability in a porous medium as quantified by the Bond and Capillary numbers. To achieve this objective, resistivity index curves were measured during the displacement of mineral oil by water in a 2D tank packed with glass beads. Four-wire resistance measurements were collected throughout the experiment while the light transmission method was used to simultaneously monitor changes in saturation. The effect of gravity on flow instability is controlled by changing the orientation of the tank to achieve different Bond numbers. Experiments at different flow rates were conducted to control the relative importance of viscous forces by varying the capillary number.

3.3.1 Experimental setup

The fluids used in these experiments are water and mineral oil (EMD Chemicals, NJ). The properties of each fluid are given in Table 3.1. We focus on a situation where a denser fluid with low viscosity (water) displaces a less dense, more viscous fluid (mineral oil) from the bottom leading to a low viscosity ratio (0.015). Viscous fingering is therefore possible in this system. Negrosine dye was added to the water phase to provide contrast with the clear mineral oil to allow visual tracking of the

displacement front and the development of fingers. This particular dye was selected because it did not partition from the water to oil phase in initial static tests conducted in beakers.

Table 3.1 Fluid Properties

Wetting phase ,water (with 0.05g/L Nigrosine)	
Density, ρ_w	1000 kg/m3
Dynamic Viscosity, μ_w	1.002E-3 N.s/m^2
Non-wetting phase, mineral oil	
Density, ρ_n	880 kg/m3
Dynamic Viscosity, μ_n	0.068 N.s/m^2
Interfacial tension, γ	0.049 N/m (Yoon,.et al, 2009)
Viscosity Ratio, M	0.015

Table 3.2 Tank Properties

Lengh×width×height, L×W×H	55cm×55cm×3.75cm
Porosity, ε	0.28
Formation factor, F_f	3.04
Permeability, k	5.63E-11m^2=57 Darcy
Grain Size, D	2mm

The experiments were conducted in the specially designed 2-D Acrylic tank shown in figure 3.2. The dimensions of the interior flow cell of the tank are 45cm x 40cm x 1.25cm. For all of the experiments in the study, the flow cell was packed with 2mm diameter glass beads. The entire cell was designed to be pressure sealed, thereby allowing for the tank to be oriented at arbitrary geometries. The outlet pressure of the tank was held at constant positive pressure by keeping the discharge reservoir above the tank (Figure 3.2a).

The tank could tilt to arbitrary angles so as to vary the gravity effect on flow and control the Bond number. The component of gravity acting on the flow system is determined by $g_\varphi = g*sin(\varphi)$, where g is acceleration due to gravity and φ is the angle of the tank relative to horizontal. For each experiment, water was injected into the tank at a constant rate selected to achieve a specified capillary number using a variable rate peristaltic pump (pump head: HV-07015-20, Master Flex). The displacing water phase is injected through a porous plastic plate covering the entire inlet surface of the beads to ensure the injection is uniform. The displaced oil phase is expelled from a similar outlet port at the opposite end of the flow cell. Both gravity effects, i.e., Bond number, and the flow rate, i.e., capillary number, influence the stability of flow in our experiments and can be changed independently of each other. A complete listing of tank orientations and flow rates used in the experiments is given in Table 3.3.

The bulk resistance of the tank was determined using the four-electrode method (Tagg et al., 1931, Aggelopolos et al., 2005). Two Pieces of copper mesh where anchored across the inflow and outflow of the tank to act as current electrodes. Two additional copper strips were positioned 2 cm away from each potential electrode within the tank to act as potential electrodes (Figure 2.2). A National Labs PXI system with multi-configuration matrix module (NI PXI-2530) was used to switch the polarity of the current electrodes. Prior to running the flow experiments, the flow cell was filled with a saline solution and measurements were taken to calibrate the geometric factor relating tank bulk resistance to resistivity. After packing the tank with the glass beads the formation factor in Archie's law was determined to be 3.0 for

our experiments by measuring resistance for several different solution conductivities.
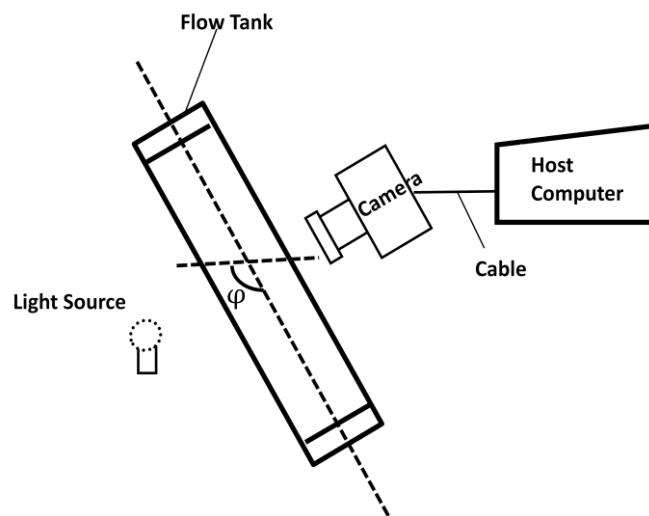
a)
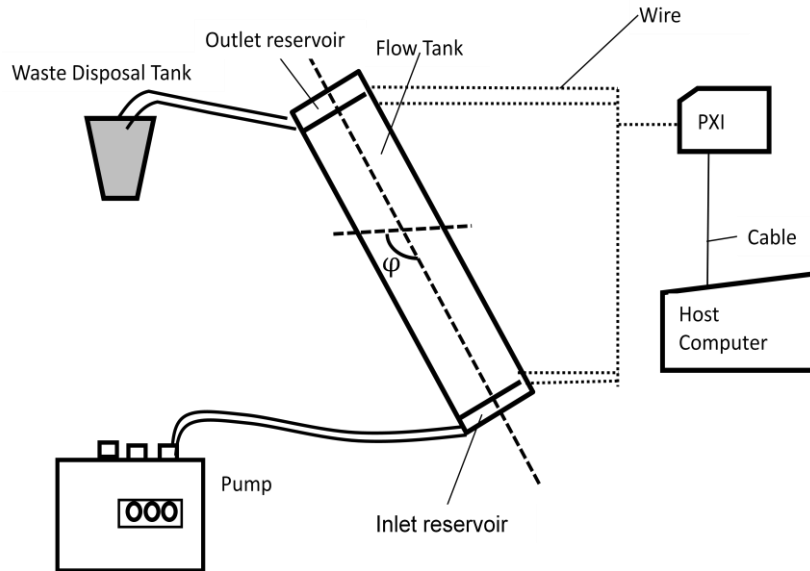
b)

Figure 3.2 Sketch of experiment setup. a) Resistivity cell, b) Light transmission

The light transmission system (Figure 3.2b) contains a light source and detector. In this experiment a scidentific digital camera is used as the detector to quantify the intensity of light transmitted through the tank. The camera is DFK 41BU02.H USB

CCD with a 5 mm lens (H0514-MP) purchased from the Imaging Source. The camera is controlled by a host computer using LabView (National Instruments) program to obtain images at a specific frame rate during the process of fluid displacement. This camera has resolution of 1280*960 pixels for 32 bit images, which provides a spatial resolution of 0.39 mm per pixel or about 2 pixels per pore for a distance between the camera and the tank of 40cm. The pictures that the camera takes are in raw bmp format with no compression. Images are later converted into gray scale and analyzed using MATLAB. The light transmitted through the tank is generated by an array of fluorescent bulbs (13W each, Bi-Pin, MA) mounted to the back of the tank in a manner allowing it to move with the tank when the experimental angle is changed.

The background reference image obtained before water is injected is subtracted from each subsequent image to overcome problems related to variations in light intensity due to the specific arrangement of light bulbs in the array. The intensity (I_0-I) of the corrected image was found to have a linear relationship with the water saturation S_w inside the porous medium:

$$S_w=[1.0759*(I_0-I)-3.3557]/100 \qquad (5)$$

This equation is obtained from calibration experiments using a small chamber with the same material, thickness and packing of glass beads to obtain a porosity of 0.28, consistent with the flow cell.

Table 3.3 summary of the inclination angles (φ) and pumping rates (Q) for each of the 34 experiments. The corresponding characteristic numbers C_a, B_o and B_o^* are also given.

Index	1	2	3	4	5	6	7
Q(ml/min)	189	251	67	119	157	27	67
φ(degree)	90	90	90	90	90	90	90
σ_w(μs/cm)	98	93	90.2	93.7	81.4	126	94.7
B_o	1.65E-02	1.65E-02	1.65E-02	1.65E-02	1.65E-02	1.65E-02	1.65E-02
C_a	1.39E-01	1.85E-01	4.94E-02	8.78E-02	1.16E-01	1.99E-02	4.94E-02
Bo*	-1.23E-01	-1.69E-01	-3.30E-02	-7.13E-02	-9.94E-02	-3.47E-03	-3.30E-02

Index	8	9	10	11	12	13	14
Q(ml/min)	119	27	189	251	358	67	99
φ(degree)	90	90	90	90	90	90	90
σ_w(μs/cm)	82	78.7	79.5	76.7	78.4	80.1	83.1
B_o	1.65E-02	1.65E-02	1.65E-02	1.65E-02	1.65E-02	1.65E-02	1.65E-02
C_a	8.78E-02	1.99E-02	1.39E-01	1.85E-01	2.64E-01	4.94E-02	7.30E-02
B_o^*	-7.13E-02	-3.47E-03	-1.23E-01	-1.69E-01	-2.48E-01	-3.30E-02	-5.66E-02

Index	15	16	17	18	19	20	21
Q(ml/min)	89	52	146	119	67	27	67
φ(degree)	90	90	90	90	90	90	90
σ_w(μs/cm)	74.8	77.6	74.2	79	77.6	78.3	87
B_o	1.65E-02	1.65E-02	1.65E-02	1.65E-02	1.65E-02	1.65E-02	1.65E-02
C_a	6.57E-02	3.84E-02	1.08E-01	8.78E-02	4.94E-02	1.99E-02	4.94E-02
B_o^*	-4.92E-02	-2.19E-02	-9.13E-02	-7.13E-02	-3.30E-02	-3.47E-03	-3.30E-02

Index	22	23	24	25	26	27	28
Q(ml/min)	189	251	67	67	67	67	67
φ(degree)	90	90	30	30	30	0	45
σ_w(μs/cm)	71.8	72.8	78	91.5	90	81.1	80.5
B_o	1.65E-02	1.65E-02	8.23E-03	8.23E-03	8.23E-03	0.00E+00	1.16E-02
C_a	1.39E-01	1.85E-01	4.94E-02	4.94E-02	4.94E-02	4.94E-02	4.94E-02
B_o^*	-1.23E-01	-1.69E-01	-4.12E-02	-4.12E-02	-4.12E-02	-4.94E-02	-3.78E-02

Index	29	30	31	32	33	34	
Q(ml/min)	67	67	67	67	358	358	
φ(degree)	15	60	60	60	90	90	
σ_w(μs/cm)	82.8	84	79.2	84.7	89.1	88.5	
B_o	4.26E-03	1.42E-02	1.42E-02	1.42E-02	1.65E-02	1.65E-02	
C_a	4.94E-02	4.94E-02	4.94E-02	4.94E-02	2.64E-01	2.64E-01	
B_o^*	-4.52E-02	-3.52E-02	-3.52E-02	-3.52E-02	-2.48E-01	-2.48E-01	

3.3.2 Summary of all experiments

With the experimental setup described above, 2 main series of 34 experiments are conducted: one series is at constant Bond number of 0.0165 and the other is at constant capillary number of 0.0494. Table 3.3 summarizes the experimental conditions for all experiments: orientation of the tank (φ), pumping rates (Q), water conductivity (σ) and the corresponding Capillary number (C_a), Bond number (B_o), and generalized Bond number B_o^*.

3.4 Results

The range of magnitudes of Bond number that can be achieved by rotating the tank, i.e., 0 to 0.0165, is smaller than the range of capillary number that can be achieved by changing the flow rate, i.e., 0 to 0.264. Therefore, we can obtain the largest range of generalized Bond numbers by changing flow rate. The maximum generalized Bond number used in the experiments is -0.0035 because the digital multi-meter was not able to read the high resistivity of the mineral oil in completely stable situations where water uniformly displaced the oil. The lowest (i.e., most negative) generalized Bond number investigated is -0.248 as the glass beads tended to compact under high internal pressures if higher flow rates were applied in the closed cell.

3.4.1 Saturation and resistivity index

The average water saturation and resistivity index of the tank over time are shown in Figure 3.3 for different values of the generalized Bond number. Saturations change

relatively smoothly in most cases as water displaces the oil. Differences between the curves are apparent, but trends for different generalized Bond number are not clear. In contrast, the resistivity index curves show a distinctive change in behavior with generalized Bond number. For small values of B_o^*, i.e., values near zero where flow is more stable, the resistivity index curves show large, sudden drops. In contrast, for large negative values of B_o^*, in which case the flow is highly unstable with many thin fingers formed, the reduction in resistivity index over time is smooth and regular. This result is indicative of the high sensitivity of resistivity measurements to the geometry of the water phase in the medium. Note that we use resistivity index here since the fluid resistivity varied between some of the experiments (Table 3.3).
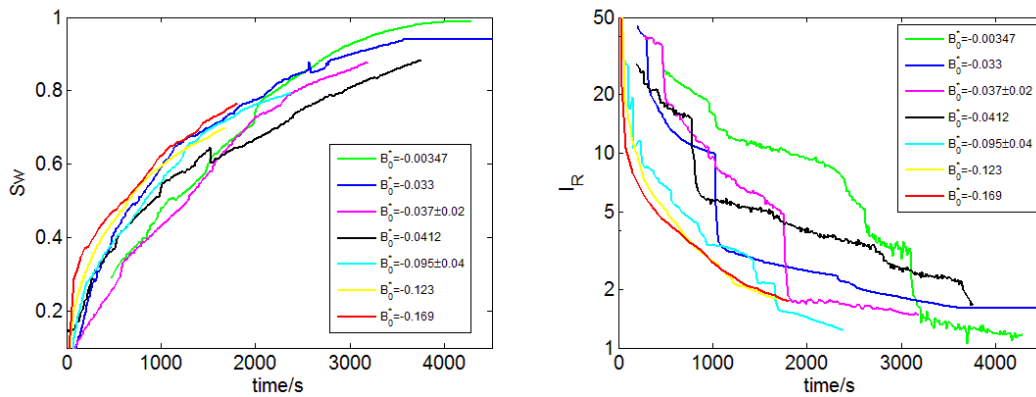

Figure 3.3 a) Average tank saturation and b) resistivity index through time for varying values of B_o^* (experiment index= 9, 7, 28, 25, 17, 10, 11)

At small negative values of B_o^* the flow is stable and the water advances either as a uniform front or as large, individual fingers. Using the video collected during the experiment, the jumps in resistivity index can be correlated to the time at which the large individual fingers of water reach the tank's upper current electrode, completing a new pathway for current flow through the medium. At large negative values of B_o^* the flow is highly unstable, producing many thin fingers. The fingers tend to reach

26

the tank outflow in a more uniform manner, producing the relatively smooth change in resistivity observed in Figure 3.3b. The patterns of fingering observed in our experiments (Figure 3.4), i.e., increasing number of fingers and decreasing finger thickness with increasing generalized Bond number, is consistent with observations from experiments by Løvoll et al. (2005) and Méheust et al. (2002) though these authors did not measure resistivity.
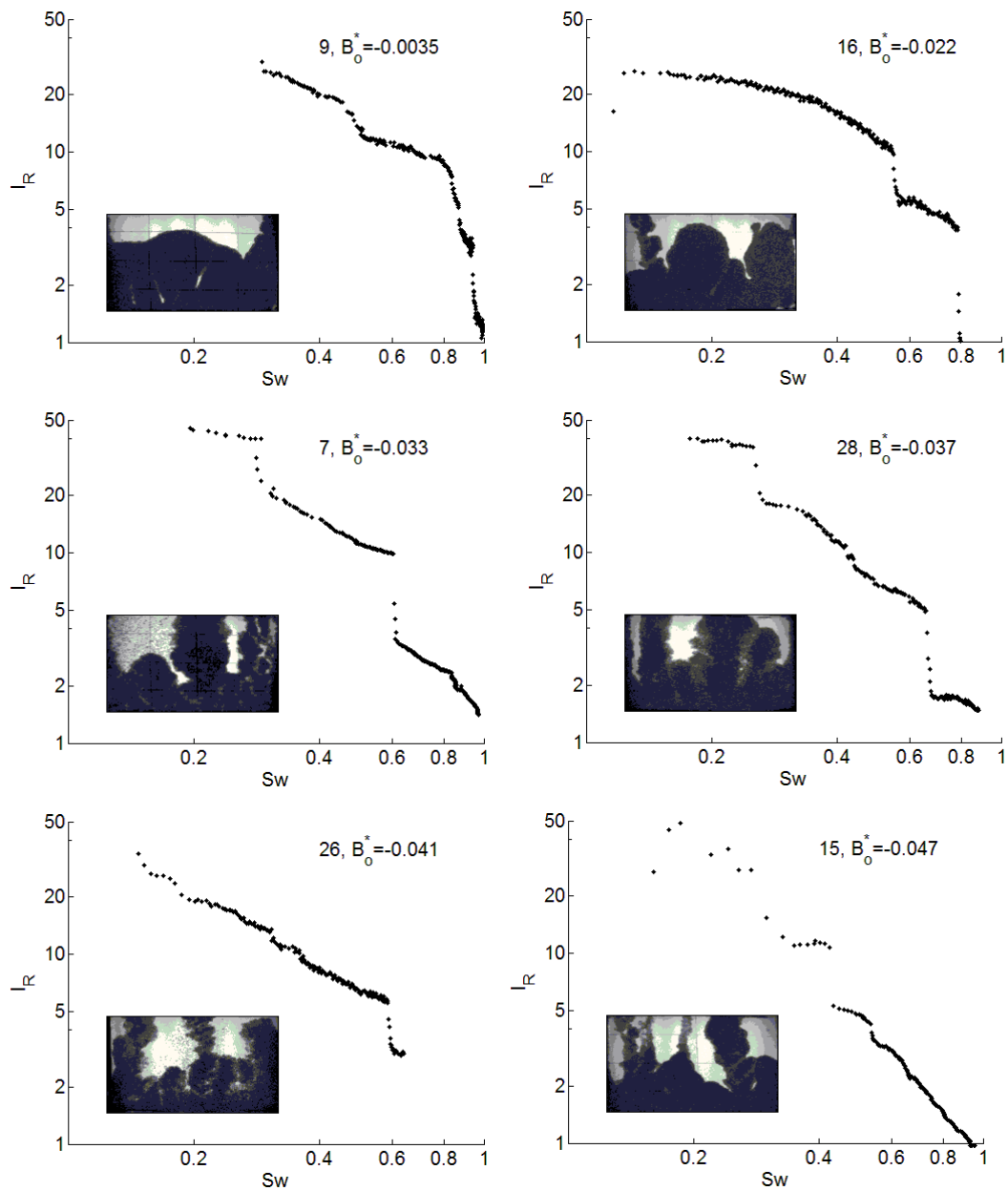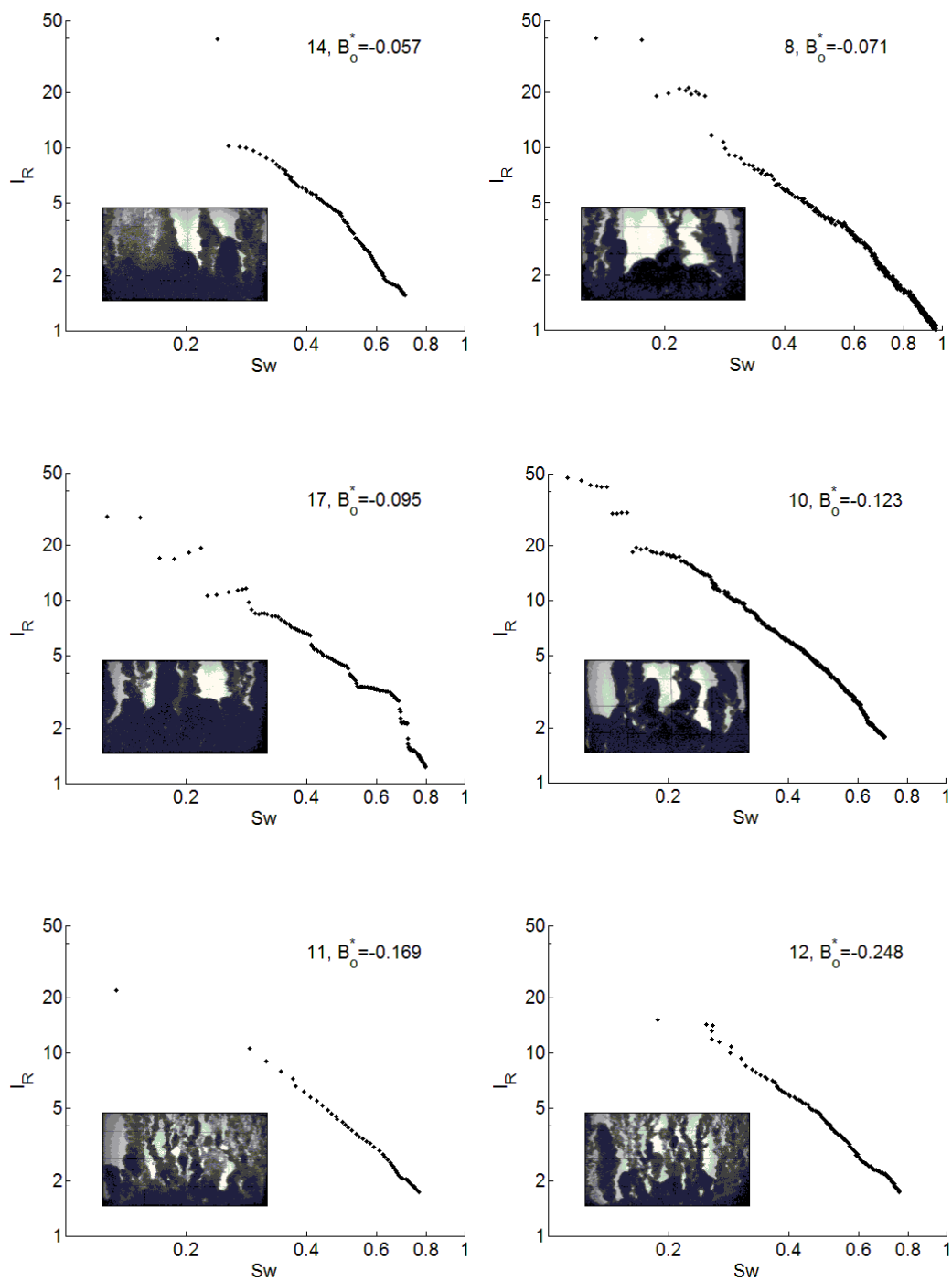
Figure 3.4 Resistivity index with saturation when varying B_o^*, for all the experiments, the B_o^* are -0.0035, -0.022, -0.033, -0.037, -0.041, -0.047, -0.057, -0.071,-0.095, -0.123 -0.169, -0.248. The inserted number in the plots refers to the index in table 3. The picture at the lower left corner represents the tank (L×45cm), L is the distance between the potential electrodes.
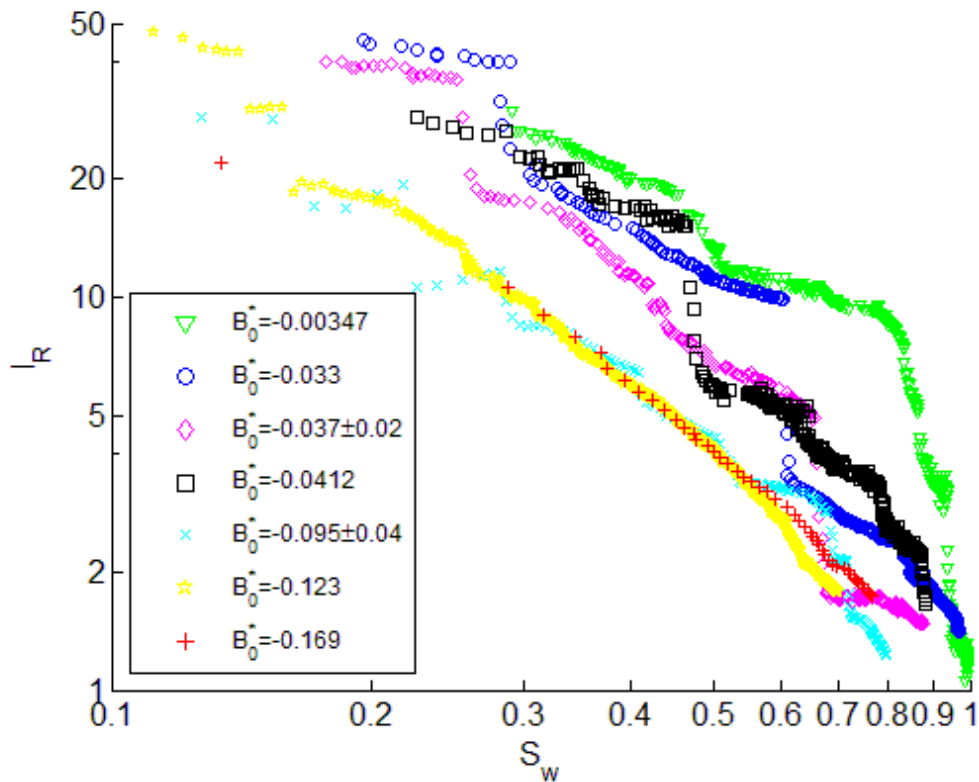
Figure 3.5 Comparison of resistivity index with different generalized Bond number

Figure 3.5 shows the resistivity index versus water saturation for a subset of the generalized Bond numbers used in the experiments. A clear trend is apparent as for a given saturation value the resistivity index is lowest for unstable flow scenarios, i.e., the value of the generalized Bond number of the curves decreases from the top curve to the bottom. The slope of the resistivity index curves is flattest for small values of the generalized Bond number with changes in resistivity occurring as sharp drops when individual fingers reach the outflow end of the tank. The magnitude of this resistivity index drop decreases as the generalized bond number decreases and disappears when the flow is very unstable at $B_o*=-0.123$ (Figure 3.5). When the generalized Bond number decreases, the fingering front width also decreases (Figure 3.7). Based on experimental data Méheust et al. (2002) suggest a power law with an

29

exponent of -0.55 to relate the width of the fingering front and the generalized Bond number (Eq.7).

$$W=B_o*^{-0.55} \qquad (6)$$

Here W is the measured front width of the finger. Therefore bigger individual drops in the resistivity index at small values of the generalized Bond number can be attributed to the wider fingers reaching the electrodes and causing a larger portion of the flow cell to connect the electrodes. As the flow grows increasingly unstable, the conductive fingers have a smaller width and distribute in the tank more uniformly. As a result, the significance of the resistivity change that is caused by an individual finger is negligible and is too small to be identified in this situation. The resistivity index versus saturation curves for unstable flow at $B_o*=-0.123$ (Figure 3.5, yellow pentagram) and $B_o*=-0.169$ (Figure 3.5, red plus), overlap with each other. At higher generalized Bond numbers, e.g., $B_o*=-0.00347$, the flow is more stable causing a very sharp drop in I_R at the end of the experiment, because the front of the water moving to the end the tank relatively flat, and much wider than other finger occurs in other experiments. In this case, both the water saturation and resistivity index are 1 at the end, indicating that the porous medium is fully saturated with water, and the resistivity of the tank is the resistivity of water.

3.4.2 Saturation exponent

If we convert Archie's Law into log scale, it is:

$$log(I_R)=-n*log(S_w) \qquad (7)$$

so water saturation is linearly proportional to resistivity index on a log scale with the slope equal to $-n$. We use this slope to calculate the saturation exponent from the measured resistivity index versus water saturation curves. For each experiment, the slope of the resistivity index-saturation curve may change as a function of saturation (Figure 3.5, 3.6). This effect is a result of the fact that the measurements represent the dynamic behavior of the flow as preferential flow paths are established within the tank. Therefore, the saturation exponent was estimated for each section of the resistivity-saturation curve, ignoring the sudden drops in resistivity caused by water breakthrough (Figure 3.6). Table 4 shows the saturation exponents estimated for each section of the curve for the experiments which have resistivity drops. We take the average of the slopes found for a curve to estimate a saturation exponent corresponding to each generalized Bond number. For the experiments with low B_o*, which is a continuous line, the saturation exponent is the reciprocal of the slope of S_w-I_R at log scale.
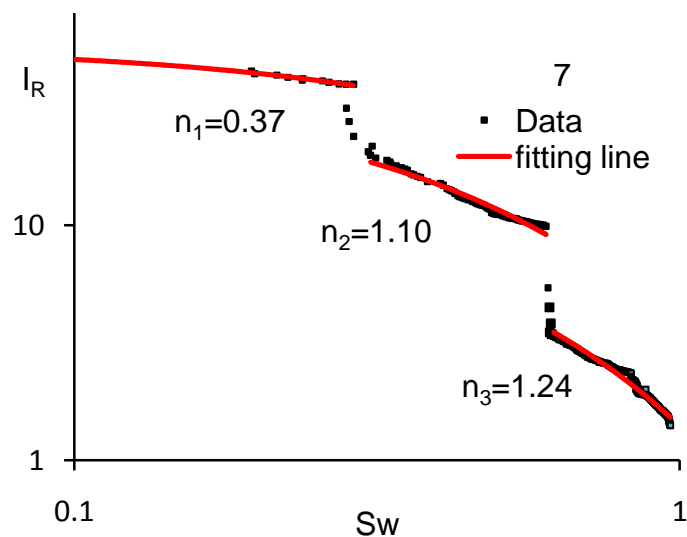

Figure 3.6 Exponential relationship between saturation and resistivity index, the reciprocal of n is the slope of each part at log scale

Table 3.4 Saturation exponent for experiments exhibiting significant resistivity drops, the index refers to table 3.3

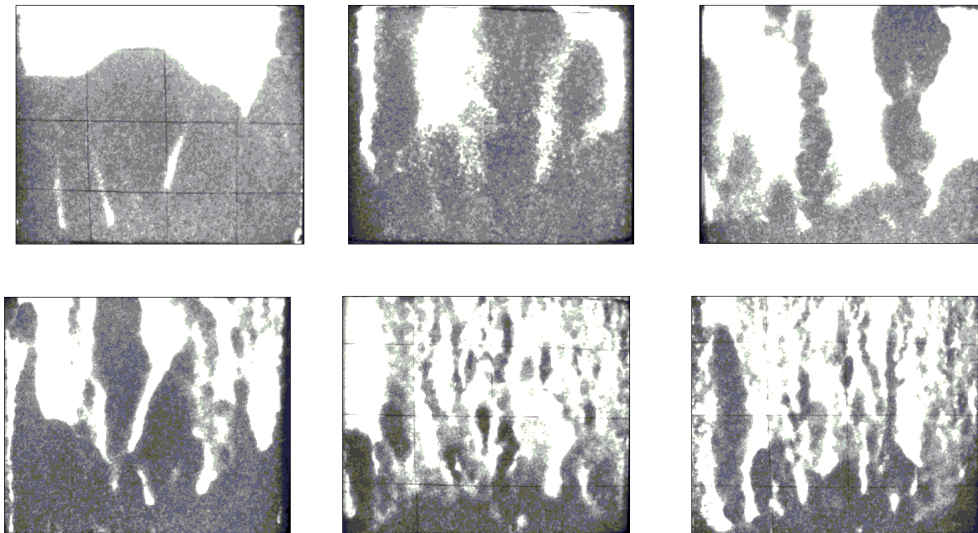| Index	Section of I_R-S_w curve		
	n_1	n_2	n_3
1	0.97	0.95	
6	0.57	0.60	
7	0.37	1.10	1.24
9	0.94	0.65	
13	0.98	0.65	
16	0.77	1.05	
18	0.98	1.93	

Figure 3.7 The picture shows how the connectivity increases with negative generalized Bond number. The B_o* are -0.0035, -0.037, -0.041, -0.071, -0.169, -0.248. The index of these pictures is 9, 28, 24, 18, 11 and 12 refers to table 3.

We find that the saturation exponent increases when B_o* decreases (Figure 3.8). It reaches a constant value of 1.94 when generalized Bond number is less than -0.106 (Figure 3.8). We generalize this relationship as follow:

$$n= -11.7*B_0^*+0.7 \qquad \text{for } -0.106<B_0^*<-0.00347$$

$$n=1.94 \qquad \text{for } B_0^*<-0.106 \qquad\qquad (8)$$

This equation shows that the connectivity, which is related with conductivity from one side of the tank to the other side, increases with B_o^*. The connection through pores is increasing with generalized Bond number when $-0.106<B_o^*<-0.00347$. The connectivity of experiments 11 and 12 are similar which cause the same saturation exponent. Further quantification of the connectivity needs to be done to prove the results.
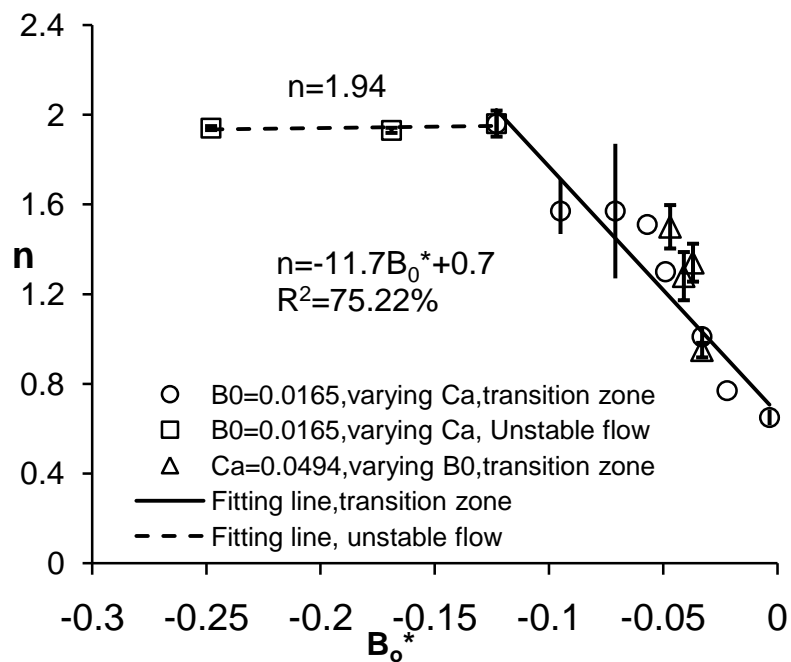

Figure 3.8 Saturation exponent as a function of generalized bond number B_o^* for all experiments with a R^2 of 75.22%

3.5 Conclusion

The displacement of water phase into a light mineral oil phase in a homogeneous porous medium using electrical resistivity method is studied experimentally. The

experimental setup allows us to change the effect of gravity by tilting the orientation of the flow. To alter viscous effects, we performed experiments with different flow rates. We use the generalized Bond number, which is the combination of gravity and viscous effect to quantify the flow condition and saturation exponent to represent the electrical resistivity property of the flow channeling. We observe a transition zone between stable and unstable displacement. We found that the saturation exponent and generalized Bond number as a linear relationship. And the saturation exponent becomes constant with a value of 1.94 when the flow is highly unstable, here when $B_o^* < -0.106$. We also observe drops of resistivity index within the transition zone with varying B_o^*. The magnitude of this drop decreases when the displacement becomes more unstable, disappearing at $B_o^* = -0.123$. This is the sign of entrance to unstable flow, and below this, the electrical resistivity property will not change when decrease the generalized Bond number, since that we observe the saturation exponent is constant and the resistivity index versus saturation curves overlap with each other.

3.6 Acknowledgments

Chapter 4 Conclusion

A two dimensional flow cell is constructed to measure the electrical properties of the multiphase flow under varying flow conditions in a homogeneous porous medium. The generalized Bond number which describes the balance between viscous, capillary, and gravity forces that affect flow instability is controlled by tilting our flow cell orientation and changing flow rate of water pumped in. The resistivity index and water saturation in the process of drainage is measured using 4-wire resistance and light transmission measurements. The saturation exponent is calculated by the relation of real time resistivity index and water saturation at varying generalized Bond number. An approximate relationship is developed for saturation exponent as a function of generalized Bond number. The most important conclusions are outlined below:

- The water residual saturation in the tank increases with flow fingering grows. When decreasing the generalized Bond number, which means the flow becomes more unstable, the residual oil saturation increases when the flow reaches equilibrium and this reducing the efficiency of oil production.
- Under the change of effects from capillary force, viscous force and gravity on the displacement pattern, the resistivity index is decreasing with time when the destabilization is growing. A big drop occurs when a water flow fingering arrive at the other end of the tank. The magnitude of this drop decreases when the flow displacement becomes more unstable and disappears when $B_0^* < -0.123$.
- The water saturation with corresponding resistivity index curves indicates that the resistivity index decreases with water saturation increase and they have linear relationship with one negative slope when one flow fingering expand from one side

of the tank to the other end. The resistivity index decreases sharply when this fingering reaches the potential electrode of the other side since the current finds a short path. The resistivity starts to decrease with saturation increase again with another negative slope. For high generalized Bond number, which represents relatively stable flow, the resistivity decreases a lot and both resistivity index and saturation are 1 at the end of experiment.

- When $-0.106 < B_0^* < -0.00347$, the saturation exponent increases with generalized bond number decreases as the following relationship:

$n = -11.7 * B_0^* + 0.7$

In a destabilized displacement, and $B_0^* < -0.106$, the saturation exponent is constant of 1.94 and independent of the flow condition and water saturation. This indicates that the electrical resistivity property will not change when the generalized Bond number is below -0.106.

References

Aggelopolos, C., Klepetsanis, P,. Theodoropoulou, M.A., et al., 2005, Large-scale effects on resistivity index of porous media, Journal of contaminant Hydrology, 77(4), 299-323

Archie, G. E, 1942, The electrical resistivity log as an aid in determining some reservoir characteristics. Petroleum Transactions of AIME 146: 54–62

Bauters, T. W. J., Dicarlo, D.A., and Steenhuis, T. S., 1998, Preferential flow in water-repellent sands, Soil science society of America Journal, Vol. 62, 1185-1190

Bekri, S., Howard, J., Muller, J., and Adler, P. M., 2003, Electrical resistivity index in multiphase flow through porous media, Transport in porous media, 51, 41-65.

Blunt M. J., Jackson, M. D., Piri, M., and Valvatne, P. H., 2002, Detailed physics, predictive capabilities and macroscopic consequences for pore-network models of multiphase flow, Advance in water Resources, 25: 1069-1089.

Bradford, S.A., Vendlinski, R. A., Abriola, L.M., 1999, The entrapment and long-term dissolution of tetrachloroethylene in fractional wettability porous media, Water Resource Research, Vol 35, No. 10, 2955-2964

Cary, J.W., Simmons, C.S and McBride, J. F, Predicting oil infiltration and redistribution in unsaturated soils, Soil Science Society of America Journal., 53, 335-342, 1989

Catalan, L.J.J., Dullien, F.A.L., 1995, Application of gravity drainage to the recovery of residual LNAPL in homogeneous and lensed sand packs, Journal of contaminant hydrology, 18, 279-306

Christensen, N.B., Sherlock, D., and Dodds, K., 2006, Monitoring CO_2 injection with cross-hole electrical resistivity tomography, Exploration Geophysics, 37, 44-49

Darnault, C.J.G., Throop, J.A., Dicarlo, D.A., Rimmer, A., Steenhuis, T.S., and Parlange, J.-Y., 1998, Visualization by light transmission of oil and water contents in transient two-phase flow field, Journal of contaminant hydrology, 31, 337-348.

Dicarlo, D.A., Bauters, T.W.J., Steenhuis, T.S., Parlange, J.-Y., and Bierck, B.R., 1997, High-speed measurements of three-phase flow using synchrotron x-rays, Water Resources Research, Vol. 33, No. 4, 569-576.

Homsy, G.M., 1987, Viscous fingering in porous-media, Annual review of fluid mechanics, 19, 271-311

Hovadik, J.M., Larue D. K., 2007, Static characterizations of reservoirs: refining the concepts of connectivity and continuity, Petroleum geosciences, Vol. 13, 3, 195-211

Klute, A., C. Dirksen., 1986. Hydraulic conductivity and diffusivity: Laboratory methods. p. 687–734.

Knudby, C., Carrera, J., 2004, On the relationship between indicators of geostatictical, flow and transport connectivity, Advance in water resources, 28, 405-421.

Lachhab, A., Zhang, Y., Muste, M.V.I., 2008, Particle tracking experiments in match-index-refraction porous media, Ground water, 46, no. 6: 865-872.

Lenormand, R., 1990, Liquid in porous media, Journal of Physics: Condensed Matter 2, SA79-SA88.

Lovoll, G., Meheust, Y., Maloy, K.H., Aker, E., Schmittbuhl, J., 2005, Competition of gravity, capillary, and viscous forces during drainage in a two-dimensional porous medium, a pore scale study, Energy, 30, 861-872.

Man, H.N and Jing, X.D., 2000, Pore network modeling of electrical resistivity and capillary pressure characteristics, Transport in porous media, 41, 263-286.

Mark., D.F, Color Appearance Models, 2nd Ed., Wiley-IS&T, Chichester, UK (2005). ISBN 0-470-01216-1

Meheust, Y., Lovoll, G., Maloy, K.J., and Schmittbuhl, J., 2002, Interface scaling in a two-dimensional porous medium under combined viscous, gravity, and capillary effects, Physical Review 66, 051603-1 – 051603-12.

Moss, A.K., Jing, X.D., et al., 2002, Wettability of reservoir rock and fluid system from complex resistivity measurements, Journal of petroleum science and engineering, 33, 75-85

Mogensen, K., Stenby, E.H., 2001, Studies of waterflooding in low-permeable chalk by use of X-ray CT scanning, Journal of Petroleum Science and Engineering, 32,1-10

Niemet, M.R., Selker, J.S., 2001, A new method for quantification of liquid saturation in 2D translucent porous systems using light transmission, Advanced in Water Resources, 24, 651-666

Oostrom, M., Dane, J.H., and Wietsma, T.W., 2007, A review of multidimensional, multifluid, intermediate-scale experiment: flow behavior, saturation imaging, and tracer detection and quantification, Vadose Zone Journal, Vol. 6, No.3, 610-637

Rimmer, A., Parlange, J.Y., et al., 1996, Wetting and nonwetting fluid displacements in porous media, Transport in porous media, 25, 205-215

Schroth, M.H., Istok, J.D., Ahearn, S.J., Selker, J.S., 1995, Geometry and position of light non-aqueous-phase liquid lenses in water-wetted porous media, Journal of contaminant hydrology, 19, 269–287

Stokes, J.P., Weitz, D.A., et al., 1986, Interfacial stability of immiscible displacement in porous medium, Physical review letters, Vol. 57, No. 14, 1718-1721

Sweeney, S.A. and Jennings Jr, H.Y., 1960, Effet of wettability on the electrical resistivity of carbonate rock from a petroleum reservoir, Journal of physical chemistry, 64, 551-553

Tagg, G.F., 1931, Prcatical investigations of the earth resistivity method of geophysical surveying, Proceedings of the physical society, 43, 305-323

Tiab, D., and Donaldson, E.C., 2004, Petrophysics-Theory and Practice of Measuring Reservoir Rock and Fluid Transport Properties, 2nd Edition

Villaume, J. E., 1985 Investigation at sites contaminated with dense nonaqueous phase liquids, Ground water monitoring Review, 5, 60-75.

Weisbrod, N., Niemet, M.R., Selker, J.S., 2002, Imbibition of saline solution into dry and prewetted porous media, Advances in water resources, 25, 841-855.

Wilson, A., 1988, What color is color? The electronic system design magazine, January, 38-44

Yoon, H., Oostromm, M., 2009. Estimation of Interfacial Tension between Organic Liquid Mixtures and Water, Environmental Science and technology, 43, 7754–7761

Zhang, Z.F., Smith, J.E., 2002, Visualization of DNAPL fingering processes and mechanism in water-saturated porous media, Transport in porous media, 48, 41-59.

Zhou, D.G., Arbabi, S., et al., 1997, A percolation theory study of wettability effect on the electrical properties of reservoir rocks, Transport in porous media, 29, 85-98

Appendices

Appendix A Measure the permeability of the formation: Falling-head method

The movement of fluid through porous medium depends on the property of the fluids such as density and viscosity, property of the formation like porosity, pore size, connectivity among the pores and hydraulic gradient. Hydraulic conductivity is a parameter to quantify the hydraulic property of the formation. To generalize the property of the fluid and the formation, we use permeability. Falling-head method (Klute et al., 1986) is used to measure the hydraulic conductivity of our medium. Permeability and hydraulic conductivity has the following relationship:

$$k=\frac{K.\mu}{\rho.g}$$

Where k is permeability, K is hydraulic conductivity of the layer which is 0.00055m/s measured from Falling-head method, μ is viscosity of fluid, we use water in our experiment which is 1.002E-3N s/m^2 at 20°C, ρ is the density of fluid, water's density at 20°C is 998.2kg/m3, g is the acceleration due to the gravity which is 9.8m/s^2.

k=5.63E-11m^2=57Darcy

Appendix B Resistivity index versus saturation when varying B_0*

For all the experiments, the inserted number in the plots refers to the index in table 3.3. The generalized Bond number can be found in table 3.3 referring to the index. The picture at the lower left corner represents the tank (L×45cm), L is the distance between the electrodes.

18

19

29

31

32

33